Title

Fabrication of centimeter-scale and geometrically arbitrary vascular networks using in vitro self-assembly

Authors

Morgan, Joshua T
Shirazi, Jasmine
Comber, Erica M
et al.

Publication Date

2019

DOI

10.1016/j.biomaterials.2018.10.021

Peer reviewed

HHS Public Access

Author manuscript

Biomaterials. Author manuscript; available in PMC 2020 January 01.

Published in final edited form as:

Biomaterials. 2019 January ; 189: 37–47. doi:10.1016/j.biomaterials.2018.10.021.

Fabrication of centimeter-scale and geometrically arbitrary vascular networks using *in vitro* self-assembly

Joshua T. Morgan[#1,†], **Jasmine Shirazi**[#1], **Erica M. Comber**[1], **Christian Eschenburg**[1], and **Jason P. Gleghorn**[1,*]

[1]Department of Biomedical Engineering, University of Delaware, Newark, DE 19716

[#] These authors contributed equally to this work.

Abstract

One of the largest challenges facing the field of tissue engineering is the incorporation of a functional vasculature, allowing effective nourishment of graft tissue beyond diffusion length scales. Here, we demonstrate a methodology for inducing the robust self-assembly of endothelial cells into stable three-dimensional perfusable networks on millimeter and centimeter length scales. Utilizing broadly accessible cell strains and reagents, we have rigorously tested a state space of cell densities (0.5-2.0×10^6 cell/mL) and collagen gel densities (2-6 mg/mL) that result in robust vascular network formation. Further, over the range of culture conditions with which we observed robust network formation, we advanced image processing algorithms and quantitative metrics to assess network connectivity, coverage, tortuosity, lumenization, and vessel diameter. These data demonstrate that decreasing collagen density produced more connected networks with higher coverage. Finally, we demonstrated that this methodology results in the formation of perfusable networks, is extensible to arbitrary geometries and centimeter scales, and results in networks that remain stable for 21 days without the need for the co-culture of supporting cells. Given the robustness and accessibility, this system is ideal for studies of tissue-scale biology, as well as future studies on the formation and remodeling of larger engineered graft tissues.

Keywords

vasculogenesis; endothelial cell; self-assembly; perfusion; multiscale; tissue engineering

[*]Address correspondence to J.P.G.: 161 Colburn Lab, Newark, DE 19716, Tel: 302-831-4836, gleghorn@udel.edu.
(†) Current address: Department of Bioengineering, University of California, Riverside

Disclosure: The authors confirm that there are no known conflicts of interest associated with this publication and there has been no significant financial support for this work that could have influenced its outcome.

Data availability

The raw/processed data required to reproduce these findings cannot be shared at this time as the data also forms part of an ongoing study.

Introduction

Large-scale loss of tissue, whether due to trauma, ischemic events, or necrotizing diseases, presents an ongoing challenge to tissue engineering and regenerative medicine. Tissue grafts have become a popular choice for replacing tissue and show promise for becoming a major therapeutic option. However, as the size of the tissue graft grows, it faces diffusion-limited nutrient and oxygen transport, which hinders cellular growth, migration, and survival within the graft. One way to overcome this barrier is to incorporate vascular and lymphatic networks into the grafts [1-4]. Indeed, vascularization of engineered graft tissue remains one of the critical challenges facing clinical translation in tissue engineering. To address these compelling issues, there is a need for a robust large-scale and physiologically representative vascularization model.

Research focused on vascularizing grafts has resulted in numerous reports of *in vitro* vascularization models, which can be fit into two broad categories: patterned and self-assembled. In patterned systems, fluid networks are patterned into a biomaterial using molding [5-8], needles [9,10], sacrificial casts [11,12], or laser-based degradation [13,14]; and endothelial cells are allowed to invade or are perfused into the network. In many of these cases, the available geometries are constrained by fabrication technique to be planar and/or restricted to straight lines, with a few notable exceptions that support arbitrary, fully three-dimensional networks [14,15]. For self-assembly models, vascular endothelial cells or progenitor cells are initially seeded within or adjacent to a three-dimensional biological or synthetic polymer matrix that supports invasion and proliferation of cells arbitrarily throughout the bulk. Typical materials include alginate [16], fibrin [17-23], collagen [24-34], collagen/fibrin [35,36], or modified PEG gels [37]. The cells then invade the surrounding matrix, create lumens through vacuole formation/coalescence, and sprout into the matrix to form an interconnected network of endothelialized tubes [38,39]. A key feature of self-assembly is that it closely recapitulates the *in vivo* processes of vasculogenesis and angiogenesis [38,39], especially in comparison to patterned models [40].

Whereas both the patterned and self-assembly methods have provided viable model systems to ask scientific questions on biochemical and biomechanical signaling in vasculogenesis and angiogenesis, cell-cell and cell-matrix interactions, and fundamental endothelial cell biology, existing systems have numerous limitations. Patterned systems, especially capillary scale networks, may be difficult to fully endothelialize [41], and the endothelial layers can be unstable after extended culture [42]. Conversely, self-assembled systems may suffer from contraction of the overall culture [27,32,43], resulting in dramatic changes to the material and boundary conditions of the culture and altering cell behavior [43-45]. Additionally, self-assembled vascular networks are prone to destabilize after only a few days [17,27,32,35,46] or require co-culture with specific non-endothelial cells (e.g. mesenchymal stem cells, pericytes) to stabilize the network [13,17-21,27,32,34,37,46,47]. Further, currently demonstrated patterned and self-assembled model systems are of limited scale. Indeed, these culture models are frequently formed on the sub-millimeter scale with relatively narrow windows of vessel size. Therefore, these models are not suitable for the study of phenomena that by definition occur across large length scales, such as vascular remodeling within a tissue graft that includes small arteries and veins (10^{-3} m) connected to capillaries (10^{-5} m)

as well as metabolite or gas exchange occurring across a tissue-scale (10^{-2}-10^{-1} m) graft. Finally, to add to the complexity, the staggering range of materials, methods, and culture conditions used, provides a steep barrier to entry for researchers seeking to use vascularized models for their studies.

To address these limitations, our objective was to develop a simple, robust, and scalable culture model of vascularized tissue that could serve as a basis for both *in vitro* studies and the development of tissue-scale vascularized tissues. In these studies, we rigorously determine a range of culture conditions that support vascular network formation with commonly accessible materials: human umbilical vein endothelial cells (HUVECs) and rat tail collagen I. We initially define a state space of HUVEC and collagen density, identifying optimal culture conditions for robust network formation. Further, we stringently define network characteristics for a range of conditions, identifying culture conditions useful for producing specific network morphologies, most notably demonstrating tunable average vessel size from the scale of a capillary (3-10 μm) to the scale of small veins and arteries (~0.5 mm). Additionally, we verify the formation of patent lumens, and we extend our model to arbitrary geometries and sizes, indicating a viable platform for tissue scale vascular network formation. Importantly, we also establish culture stability up to 21 days, without a requirement of mural cell co-culture. In aggregate, this study demonstrates a robust self-assembly methodology for the creation of three-dimensional, perfusable, and stably endothelialized networks on millimeter and centimeter length scales.

Materials and Methods

Collagen well/mold fabrication

Wells for the collagen gels were fabricated in polydimethylsiloxane (PDMS; Sylgard 184; Dow Corning, Midland, MI) using steel punches of the specified shape and diameter. To bond the collagen gels to the well sidewalls, the PDMS surfaces were plasma cleaned (Harrick Plasma, Ithaca, NY), immersed in 2% (poly)ethylenimine (PEI) for 30 minutes, rinsed three times with deionized water, dried, immersed in 0.2% glutaraldehyde (GA) for 1 hour, and again rinsed and dried, similar to prior studies [28]. The functionalized PDMS wells were then placed on appropriately sized glass cover slips that lacked surface treatment. Collagen gels were formed in these wells, which thus served as gelation molds, and the PDMS functionalization resulted in fixed boundary conditions around the perimeter of the gels and the non-treated glass coverslip and open top resulted in upper and lower surfaces that were free to slip (Figure 1A).

Collagen isolation

Collagen was isolated from rat tail tendons similar to previous descriptions [28,48,49]. Briefly, tendons were removed from rat tails (Pel-Freez Biologicals, Rogers, AR) and left to soak in 1X DPBS. The isolated collagen was then transferred into acetone for 5 minutes, followed by 70% isopropanol for an additional 5 minutes. The fibers were then dissolved in 0.1% glacial acetic acid at 4°C for 48 hours. Dissolved collagen was centrifuged at ~28,000×*g* for 2 hours to remove impurities. The resulting supernatant was frozen at −80 °C

overnight and lyophilized to generate a collagen sponge. The resulting sponge was dissolved into stock solutions (6-10 mg/mL) in 0.1% glacial acetic acid and stored at 4°C.

Gel fabrication and mechanical characterization

Collagen gels were fabricated similar to previous work [24-34]. Briefly, the acidic collagen stocks were diluted to the specified concentrations in 10X HBSS (final concentration 1X; ThermoFisher, Waltham, MA) and Endothelial Cell Growth Medium-2 (EGM-2; Lonza, Walkersville, MD) on ice. Next, 1N NaOH was used to neutralize pH, and the collagen suspension was immediately pipetted into the molds and transferred to a 37°C incubator for gelation. For mechanical characterization, 3mm thick acellular gels were formed in 8 mm diameter molds that were not surface treated and transferred to a DHR-3 Discovery Hybrid Rheometer (TA Instruments, New Castle, DE) for testing. Collagen gel mechanical properties were assessed using a strain sweep at constant frequency (ε = 0.1-100%; f = 1 Hz) and a frequency sweep at constant strain (f = 0.01 - 100 Hz; ε = 10%). Values were consistent with previously reported rheological studies of rat tail collagen [50–52] (Figure 1B).

Cell culture and construct fabrication

Human umbilical vein endothelial cells (HUVECs, ATCC, Manassas, VA) were routinely cultured at 37°C and 5% CO2 in EGM-2 (Lonza). Passages 7 through 9 were used for all experiments. To ensure an endothelial phenotype at these passages, we performed Western blotting for VE-cadherin (Santa Cruz) and stained for endothelial markers PECAM1 (Cell Signaling) and VE-cadherin, observing robust expression at all passages used (Supplementary Figure 1AB), consistent with previous reports showing stable phenotype to high passage [53,54]. For suspension in the collagen gels, trypsinized cells were pelleted at 500×g and resuspended in an appropriate volume of media. The cell suspension was mixed with the collagen solution and the same procedures were used above that describe acellular collagen gel gelation. Following gelation, 2% vasculogenesis media (EGM-2 with 50 ng/mL tetradecanoylphorbol acetate (TPA; Adipogen, San Diego, CA) and 50 μg/mL sodium ascorbate) was added dropwise and changed daily. Media formulation was adapted from prior studies [28]. To ensure endothelial phenotype was maintained in 3D culture, we verified PECAM1 expression after culture in constructs that represent different extremes in collagen density and cell number (Supplementary Figure 1CD). Except when noted otherwise, culture duration was 7 days.

Fixation and imaging

Following culture gels were washed 3 times with 1X DPBS and fixed in 4% paraformaldehyde supplemented with 0.1% Triton-X for 2 hours at 4°C. Following fixation, the gels were washed three times in 1X DPBS and stained with 500 ng/mL DAPI (ThermoFisher Scientific, Waltham, MA) and CF594 conjugated phalloidin (Cell Signaling Technologies, Danvers, MA)), at a 1:200 dilution at 4°C overnight. The gels were again washed three times with 1X DPBS and stored hydrated until imaging. Gels were imaged on a Zeiss widefield AxioObserver Z1 for gross characterization and a Zeiss confocal LSM880 for reflectance and detailed fluorescence analysis. Widefield images of the entire gel area were assessed to determine the extent of network formation and scored by 6 masked

observers as follows: 1 = no proliferation, 2 = clusters only, 3 = clusters (75%) and network (25%), 4 = clusters (50%) and network (50%), 5 = clusters (25%) and network (75%), and 6 = network only. These scores were used to group the samples into different regions of the state diagram. Representative gels were chosen for confocal microscopy along with more rigorous analysis.

Quantitative 3D plexus analysis

For each condition, several (5-31) confocal subvolumes (each ~1 mm^3) were analyzed. A custom analysis algorithm was formulated in MATLAB (MATLAB 2015b; Mathworks, Natick, MA). Both reflectance (collagen and void space) and fluorescent (phalloidin: actin cytoskeleton; cells) confocal volumes were processed for each confocal sub-volume. In all sub-volumes, laser attenuation through the volume was compensated for via slice-by-slice histogram adjustment to low and high saturation of 5% and 0.2%, respectively. Volumes were enhanced through median filtering, phase-preserving noise removal [55], and a reconstruction implementation of tophat filtering [56]. Cells and collagen voids were segmented out of the overall volume using hysteresis thresholding [57], and cell and void volumes were combined into a ‘network’ volume. To prevent inclusion of non-cellularized void space in the network, void volume had to be contiguous with cellular volume for inclusion. The resulting volume was reduced to a skeleton using a modification of the fast marching algorithm described by van Uitert and Bittner [58].

From the network volume and skeleton, the following parameters were extracted to quantify network morphology: (1) vessel diameter; (2) vessel length between junctions; (3) junction geometry; (4) network connectivity; (5) volume fraction of the network; (6) volume fraction of void space in the network (i.e. percentage of lumenized network); (7) network coverage (i.e. fraction of overall volume with nearby network). For clarity, labeled representative images of each parameter is provided in the appropriate section of Results.

Verification of patent lumens

To verify that the vascular networks supported convective flow, we created a 4 mg/mL collagen construct seeded with 1.0×10^6 cell/mL in a $2 \times 2 \times 5$ mm^3 rectangular channel within a PDMS microfluidic device with inlet and outlet on either end of the channel. Cells were cultured as described above for 7 days, and network formation was confirmed by brightfield microscopic inspection. To visualize flow and verify patency, media with 0.1% microspheres (500 nm, Dragon Green fluorophore; Bangs Laboratories, Fishers, IN) was perfused through the vascularized gel with a syringe pump with a volumetric flow rate of 2.34 μL/min corresponding to a nominal flow velocity of 13 μm/s. Flow was visualized on a Zeiss AxioObserver Z1 widefield microscope. To highlight the functionality of the self-assembled vascular network across a range of conditions and culture durations, we generated plexus networks within cylindrical constructs (7 mm diameter, 3 mm thick) of various collagen densities and cell concentrations. Following 14 days of culture, the constructs were incubated with Vybrant Dil membrane dye for three hours to label self-assembled HUVECs. Following cell labeling, a lumen within the plexus was cannulated with a pulled glass needle connected to a syringe pump. The plexus was perfused with 2μm fluorescent microspheres

(Polystyrene Dragon Green; Bangs Laboratories, Fishers, IN). After stopping the flow, the various constructs were imaged on a Zeiss confocal LSM880 microscope.

Results

Multicellular phenotypes of HUVECs exist in three-dimensional culture

Initial experiments focused on basic validation of the three-dimensional culture methodology. HUVECs were suspended in neutralized collagen gels at a range of cell (0.5, 1.0, 1.5, 2.0 $\times 10^6$ cells/mL) and collagen (2.0, 3.0, 4.0, 5.0, 6.0 mg/mL) densities. Cultures were maintained for 7 days in vasculogenesis media (VM) as described in the Methods. After 7 days, the cells were fixed and stained with DAPI and phalloidin and imaged. In this initial screening, we observed several phenotypes and assigned scores from 1-6 with the framework detailed in the Methods, briefly: (1) no proliferation, (2) cluster formation, (3-5) clusters with some network, (6) full network. Examples of these phenotypes are shown in Figure 2A. In some cases, the gels contracted due to insufficient adhesion to the sides of the well, typically at low collagen concentrations, and given a score of 0 (data not shown).

Identification of culture conditions resulting in robust network formation

Based on our preliminary findings, we repeated cultures for all conditions (n=3-15) and imaged the entire collagen gel using automated tiling and confocal microscopy for every sample. Using a group of six masked and trained observers, each construct was viewed in its entirety, and scored from 1-6 using the scoring framework detailed in the Methods section. Collagen gels that contracted before fixation were scored 0. Each masked observer was shown every cellular collagen gel in a randomized order, and each gel was displayed in triplicate to measure observer scoring consistency. “Within observer” standard deviation was 0.58 ± 0.07 (mean ± S.E.M.), and each observer was represented by their average score. “Among observer” standard deviation was 0.59 ± 0.03 (mean ± S.E.M.), demonstrating consistency in the scoring system. Contrary to our expectations, we observed a range of culture conditions that supported robust network formation (Figure 2B). Strikingly, these lay along an axis of increasing cell and collagen density, while “off-axis” cultures failed to form consistent networks. In low cell densities and high collagen densities the failure was typically of poor proliferation or cell death, whereas high cell densities in low collagen densities resulted in rapid (1-2 days) contraction and compaction of the gels.

Quantification of vascular network morphology

Despite the fact that a range of cell/collagen density pairings resulted in robust network formation (Figure 2B, blue region bordered by black), we observed striking differences in the phenotypes of the networks depending on the culture conditions. Using confocal imaging, we obtained detailed volumetric images of a subset of cultures along the functional axis identified from qualitative scoring. Example confocal planes (Figure 3) highlight the diverging properties based on culture conditions; large, heavily lumenized vessels were typical of lower collagen densities whereas denser collagen resulted in thinner but still highly connective networks. Animations of the three-dimensional confocal volumes (Movie S1) demonstrate that the network is highly connective in three dimensions and spans the entire volume.

From these images, we employed automated segmentation of the cellular, collagen, and lumen fractions to extract metrics of network morphology. Initially, we quantified how completely the network filled the overall volume (Figure 4), using a volume fraction of the combined HUVEC and lumens compared to overall culture volume (ϕ_F) as well a metric of diffusion length (L_D). L_D was approximated by determining the Euclidean distance between each point in the collagen volume and the nearest point on the network. Reported values indicate the distance that encompasses 90% of the volume. This parameter can be used to optimize studies that rely on the diffusion of reagents such as dextran or soluble factors such as O_2. Volume fraction in general increased with increasing cell seeding density, as might be expected. However, we also observed a drop-in volume fraction with 6 mg/mL collagen, potentially due to decreased migration within the denser matrix. Increased volume fraction and decreased diffusion length would be preferable for metabolically active tissues. Additionally, we quantified branch morphology, using the segments identified by the skeletonization algorithm as “branches.” It is important to note, the skeletonization algorithm we employed does not identify any hierarchy, and therefore treats a long vessel with multiple branch points as a sequence of shorter vessels. From this, we quantified the average diameter (D_s) and tortuosity ($\tau = length/chord$; 1 indicates straight segments) for the networks (Figure 5). Overall, individual segment diameters ranged from ~5-200 μm, on the scale of the microcirculatory system, with the average diameter of segments falling within 10-25 μm for all culture conditions. Tortuosity remained consistent and close to 1 (average τ > 1.26 for all cases) regardless of condition, indicating relatively straight segments. However, as mentioned above, our analysis was limited to relatively short segments (average segment lengths ~10-40 μm) between vessel branch points, which would not identify larger scale tortuosity of the network.

Finally, we also characterized the key metrics relevant for network perfusion. We quantified network connectivity by looking at the volume fraction of the largest contiguous network (ϕ_C, volume of the largest contiguous structure divided by overall network volume) and fraction of the skeleton that is lumenized (ϕ_L, percentage of the network skeleton that intersects with lumen volume) for the confocal volumes (Figure 6). In all cases, the networks were highly connective. Lumenization was fairly consistent at ~20-30% of the overall network. Both connectivity and lumenization are important parameters for functional vascularized constructs, as they directly relate to ability to support convective flow. A disconnected, poorly lumenized network would only support localized convection, while in theory a highly connective and lumenized network would be able to support convection throughout the construct.

Functional validation of self-assembled network perfusability

Based on our confocal analysis, we observed highly interconnected and lumenized structures. To verify that these lumens were patent and able to support flow we used two methods to perfuse fluorescent microspheres through the plexus in self-assembled networks derived from a range of collagen densities and cell concentrations. First, we created a 4 mg/mL collagen construct seeded with 1.0×10^6 cell/mL that was formed within a PDMS channel (5 mm long, 2 mm wide, 2 mm deep) connecting two fluid reservoirs (Figure 7A). Culture medium was changed daily, adding the same volume of fresh medium to both

reservoirs to maintain no flow through the plexus. A self-assembled plexus was generated in this format and following seven days of culture, the resulting plexus was perfused by a syringe pump with culture media containing 500nm fluorescent beads with a nominal flow rate of 13 μm/s. Epifluorescent imaging of the majority of the construct illustrates convection of the beads throughout the network (Figure 7B), demonstrating a large-scale interconnected perfusable network. Live imaging of the flow (Figure 7C, Movie S2) demonstrates convective flow through the lumenized network. As these cellular constructs are large-scale and macroscopically thick, live imaging remains a challenge. To further confirm perfusion through the vascular lumen and not through the bulk collagen at longer durations of culture, we generated plexus networks within cylindrical constructs (7 mm diameter, 3 mm thick) of various collagen densities and cell concentrations. Following 14 days of culture, the constructs were incubated with a membrane dye to label self-assembled HUVECs. Following cell labeling, the plexus was perfused with 2μm fluorescent microspheres. After stopping the flow, the various constructs were imaged on a confocal microscope. Our results confirm the successful perfusion of large diameter vessels (Figure 7C) and the perfusion of small vessel lumens (Figure 7DE) even in constructs following two weeks of culture.

Temporal and spatial extensibility of the culture model

Given the reported challenges of long term stability of self-assembled networks and the needed co-culture of supporting cell types [13,17-21,27,32,34,35,37,46,47], we repeated one of the culture conditions in triplicate (5 mg/mL collagen, 1.5×10^6 cell/mL) and fixed cultures at 7, 14, and 21 days. We observed no loss of network or gel stability by 21 days, or any gross changes in morphology after 7 days, demonstrating suitability for long-term studies (Figure 8A). Further, we used PDMS molds of arbitrary geometry, including ‘star’ and ‘flower’ shapes, demonstrating the boundary shape has limited impact on network morphology (Figure 8B). Vascular self-assembly occurred throughout the collagen gels including at rounded edges and acute pointed edges. Finally, to demonstrate application to tissue-scale problems, we cultured plexuses in circular PDMS molds 19 mm in diameter. Despite the dramatic increase in gel diameter and volume, we still observed network formation spanning the entire culture (Figure 8C). These large networks remain lumenized and highly interconnected, which can be seen on confocal imaging (Figure 8D) of a region that roughly corresponds to the size of the dotted cyan box in Figure 8C. In aggregate, these results demonstrate the versatility and robustness of our methodology.

Discussion

Unvascularized tissue grafts, whether engineered or transplant, are limited in size to prevent necrosis of the grafted tissue. The diffusion of oxygen, nutrients, and waste through unvascularized tissue therefore remains one of the key challenges in tissue engineering. A prime example of this can be seen in the care of chronic wounds such as diabetic foot ulcers, where several engineered graft solutions have been developed, but are of limited efficacy due to a lack of vascularization [59]. There remain several fundamental knowledge gaps that prevent development of tissue-scale vascularized tissues. Numerous models have been previously created, both in clinical and basic research, spanning a range of self-assembled

and patterned techniques [5-34]. Unfortunately, these techniques often compare poorly with each other, and studies vary on how network morphology is defined, quantified, and reported. In this work, we describe an accessible methodology and state-space framework to identify a range of culture conditions for robust functional network formation and define qualitative and quantitative metrics to assess and compare self-assembled vascular network morphologies.

Previous models of vascularization have fallen into two main categories; either the endothelial cells are patterned along a predefined channel network, often described as “top-down” fabrication systems, or they are allowed to self-assemble into a network within a cell-modifiable matrix. Despite the potential demonstrated by numerous studies, the field suffers from a diversity of methodologies; biomaterials, matrix densities, media, and culture durations vary widely. Determination of the optimum culture conditions are further complicated by inconsistent quantification methods. In aggregate, this presents a challenge to researchers attempting to replicate and expand on existing work. To overcome this, we demonstrated a simple methodology for 3D culture of endothelial cells and utilized a wide range of culture conditions to identify an axis of increasing cell and collagen density that supported robust network formation (Figure 2). Importantly, we also identify culture conditions that, through a mismatch of cell and collagen densities, do not result in network formation. High densities of collagen coupled with low cell numbers results in limited proliferation and cell death without network formation. On the other hand, if the cell concentration is too high in low collagen densities, the entire matrix contracts and the stable boundary conditions on the collagen gel are not maintained likely due to the inherent contractility of the cells. Qualitative assessment of both the successful conditions and the regions of failure enables future researchers to quickly screen conditions for their work. This state-space framework is particularly useful even if biological variability shifts the axis of robust network generation for specific cell and collagen preparations.

Building upon the qualitative assessments described above, we used confocal imaging and automated segmentation to quantitatively describe the vascular networks along the axis of successful culture. A key finding of this work is that we can adjust morphology of the selfassembled network based on the starting culture conditions. Increasing cell numbers and decreasing collagen density increases volume fraction and decreases approximate diffusion distance (Figure 4), an important consideration for future experiments involving a metabolically active stroma. For example, if considering O_2 diffusion, one would ideally employ a system where the Krogh distance is greater or equal to the diffusion length, which can be significantly slower in collagen gels than in water [60] and local oxygen tension would be an important consideration for a metabolically active stromal cell population. Further, the networks are minimally tortuous with diameters consistent with the microcirculatory system (Figure 5); factors that would impact the fluid mechanics in the presence of flow. We did observe a trend of increased lumen size in the lower collagen densities, and this is likely partially attributable to increasing pore size with lower densities, although overall lumen size is significantly larger than expected pore size of 10-15 μm [28], This leads to the most important findings of this work: the high connectivity of the networks and consistent level of lumenization (Figure 6). These data suggest networks capable of supporting fluid flow, and this was verified with convective transport of fluorescent

microspheres through a network generated with 4 mg/mL and 1×10^6 cell/mL (Figure 7). These data are essential demonstrations of the functionality of the cultures, and indicate both usefulness as a research tool as well as clinical promise.

Looking ahead, this method demonstrates great potential as a robust platform for further basic science research for two key reasons. First, this method is accessible: commercial media, common cell model, and a biomaterial that requires no specialized processing. Second, due to the demonstrated robustness of the network over a range of culture conditions (Figure 2), support of convective flow (Figure 7), and the significant scalability in time and geometry (Figure 8), this culture model is adaptable to numerous studies; for example, basic vascular biology, impact of mechanical cues such as shear, and interaction of the endothelial cells with stromal cell populations. Further, as the demonstrated stability of the structure with time (Figure 8A), this method enables long-term experiments to be carried out within a 3D vascularized tissue. With further development, this could stand as an *in vitro* replacement to current *in vivo* models of tumor growth, chronic ischemic/reperfusion injury, environmental toxins, and other diseases that, by their very nature, are not amenable to traditionally brief *in vitro* studies.

There are several limitations to the model in its current form. Despite the ability to alter the geometry, it is important to note that the vasculature assembled is consistent and random across the construct, making it difficult to specifically pattern a hierarchical artery-arteriole-capillary-venule-vein network more representative of *in vivo* tissue. Additionally, while not requiring stromal or mural cells is a strength of the model in terms of simplicity, more relevant constructs would incorporate heterogeneous cell populations. Finally, although the accessibility described herein is ideal for ensuring comparability and repeatability of future *in vitro* studies across research groups, it is not directly amenable to clinical applications due to the limitations described above as well as potential immunogenicity. However, given the demonstrated ability to extend these networks to arbitrary geometries and centimeter scales (Figure 8B-D), we speculate there is great potential to treat traumatic or atrophic loss of tissue at scales currently out of reach of engineered grafts while closely matching the biological geometry. To pursue this, future studies will leverage existing technologies to accelerate clinical translation: usage of chemically-defined media, engineered collagen-mimetics or degradable hydrogels, and induced pluripotent stem cell (iPSC)-derived endothelial cells will allow the formation of vascularized graft tissue appropriate for pre-clinical and clinical studies.

Conclusion

We have demonstrated an accessible, robust model of self-assembled tissue-scale vascularization *in vitro,* and used a state-space framework to understand the relative contributions of cell number and collagen content in vascular network formation. Vascular network morphology was described qualitatively and quantitatively, demonstrating tunable vascular network properties over a range of culture conditions. The methodology is amenable to extended duration as well as arbitrary size and scale, enabling future studies in complex tissues as well as potential clinical translation.

Supplementary Material

Refer to Web version on PubMed Central for supplementary material.

Acknowledgments

The authors would like to thank Mr. Peter Sariano, Ms. Elizabeth Marcin, Ms. Meibin Chen, Ms. Julia Pelesko, Ms. Elizabeth Soulas, Mr. Daniel Minahan, and Ms. Allyson Dang for their technical and plexus scoring assistance. This work was supported in part by grants from the National Institutes of Health (R01HL133163, R21ES027962, P30GM110759, P20GM103446, U54GM104941, S10OD016361), the National Science Foundation (1537256, IGERT Traineeship 1144726 to J.S.), the University of Delaware Research Foundation, the Oak Ridge Associated Universities Ralph E. Powe Junior Faculty Enhancement Award (J.P.G.) and the March of Dimes Basil O'Connor Award (5-FY16-33 to J.P.G).

Abbreviations:

DPBS	Dulbecco's phosphate-buffered saline
EGM-2	endothelial growth media-2
GA	glutaraldehyde
HBSS	Hank's balanced salt solution
HUVEC	human umbilical vein endothelial cells
PDMS	polydimethylsiloxane
PEI	polyethylenimine
TPA	tetradecanoylphorbol acetate
VM	vasculogenesis media

References

[1]. Johnson PC, Mikos AG, Fisher JP, Jansen JA, Strategic directions in tissue engineering, Tissue Eng. 13 (2007) 2827–2837. doi:10.1089/ten.2007.0335. [PubMed: 18052823]

[2]. Montgomery M, Zhang B, Radisic M, Cardiac Tissue Vascularization: From Angiogenesis to Microfluidic Blood Vessels, J. Cardiovasc. Pharmacol. Ther. 19 (2014) 382–393. doi: 10.1177/1074248414528576. [PubMed: 24764132]

[3]. Hirt MN, Hansen A, Eschenhagen T, Cardiac tissue engineering: state of the art, Circ. Res. 114 (2014) 354–367. doi:10.1161/CIRCRESAHA.114.300522. [PubMed: 24436431]

[4]. Jain RK, Au P, Tam J, Duda DG, Fukumura D, Engineering vascularized tissue, Nat. Biotechnol. 23 (2005) 821–823. doi:10.1038/nbt0705-821. [PubMed: 16003365]

[5]. Morgan JP, Delnero PF, Zheng Y, Verbridge SS, Chen J, Craven M, Choi NW, Diaz-Santana A, Kermani P, Hempstead B, López JA, Corso TN, Fischbach C, Stroock AD, Formation of microvascular networks in vitro, Nat Protoc. 8 (2013) 1820–1836. doi :10.1038/nprot.2013.110. [PubMed: 23989676]

[6]. Zheng Y, Chen J, Craven M, Choi NW, Totorica S, Diaz-Santana A, Kermani P, Hempstead B, Fischbach-Teschl C, López JA, Stroock AD, In vitro microvessels for the study of angiogenesis and thrombosis, Proc. Natl. Acad. Sci. U.S.A. 109 (2012) 9342–9347. doi:10.1073/pnas. 1201240109. [PubMed: 22645376]

[7]. Choi NW, Cabodi M, Held B, Gleghorn JP, Bonassar LJ, Stroock AD, Microfluidic scaffolds for tissue engineering, Nat Mater. 6 (2007) 908–915. doi:10.1038/nmat2022. [PubMed: 17906630]

[8]. Verbridge SS, Chakrabarti A, DelNero P, Kwee B, Varner JD, Stroock AD, Fischbach C, Physicochemical regulation of endothelial sprouting in a 3D microfluidic angiogenesis model, J Biomed Mater Res A. 101 (2013) 2948–2956. doi: 10.1002/jbm.a.34587. [PubMed: 23559519]

[9]. Chrobak KM, Potter DR, Tien J, Formation of perfused, functional microvascular tubes in vitro, Microvasc. Res. 71 (2006) 185–196. doi:10.1016/j.mvr.2006.02.005. [PubMed: 16600313]

[10]. Price GM, Wong KHK, Truslow JG, Leung AD, Acharya C, Tien J, Effect of mechanical factors on the function of engineered human blood microvessels in microfluidic collagen gels, Biomaterials. 31 (2010) 6182–6189. doi:10.1016/j.biomaterials.2010.04.041. [PubMed: 20537705]

[11]. Golden AP, Tien J, Fabrication of microfluidic hydrogels using molded gelatin as a sacrificial element, Lab Chip. 7 (2007) 720–725. doi:10.1039/b618409j. [PubMed: 17538713]

[12]. Baker BM, Trappmann B, Stapleton SC, Toro E, Chen CS, Microfluidics embedded within extracellular matrix to define vascular architectures and pattern diffusive gradients, Lab Chip. 13 (2013) 3246–3252. doi:10.1039/c3lc50493j. [PubMed: 23787488]

[13]. Culver JC, Hoffmann JC, Poché RA, Slater JH, West JL, Dickinson ME, Three-Dimensional Biomimetic Patterning in Hydrogels to Guide Cellular Organization, Adv. Mater. 24 (2012) 2344–2348. doi:10.1002/adma.201200395. [PubMed: 22467256]

[14]. Heintz KA, Bregenzer ME, Mantle JL, Lee KH, West JL, Slater JH, Fabrication of 3D Biomimetic Microfluidic Networks in Hydrogels, Adv Healthc Mater. (2016). doi:10.1002/adhm.201600351.

[15]. Kolesky DB, Truby RL, Gladman AS, Busbee TA, Homan KA, Lewis JA, 3D bioprinting of vascularized, heterogeneous cell-laden tissue constructs, Adv. Mater. Weinheim. 26 (2014) 3124–3130. doi:10.1002/adma.201305506. [PubMed: 24550124]

[16]. Chan JM, Zervantonakis IK, Rimchala T, Polacheck WJ, Whisler J, Kamm RD, Engineering of In Vitro 3D Capillary Beds by Self-Directed Angiogenic Sprouting, PLoS ONE. 7 (2012). http://www.ncbi.nlm.nih.gov/pmc/articles/PMC3514279/ (accessed July 22, 2016).

[17]. Whisler JA, Chen MB, Kamm RD, Control of perfusable microvascular network morphology using a multiculture microfluidic system, Tissue Eng Part C Methods. 20 (2014) 543–552. doi: 10.1089/ten.TEC.2013.0370. [PubMed: 24151838]

[18]. Carrion B, Huang CP, Ghajar CM, Kachgal S, Kniazeva E, Jeon NL, Putnam AJ, Recreating the perivascular niche ex vivo using a microfluidic approach, Biotechnol. Bioeng. 107 (2010) 1020–1028. doi:10.1002/bit.22891. [PubMed: 20672286]

[19]. Ghajar CM, Blevins KS, Hughes CCW, George SC, Putnam AJ, Mesenchymal stem cells enhance angiogenesis in mechanically viable prevascularized tissues via early matrix metalloproteinase upregulation, Tissue Eng. 12 (2006) 2875–2888. doi:10.1089/ten.2006.12.2875. [PubMed: 17518656]

[20]. Ghajar CM, Chen X, Harris JW, Suresh V, Hughes CCW, Jeon NL, Putnam AJ, George SC, The effect of matrix density on the regulation of 3-D capillary morphogenesis, Biophys. J. 94 (2008) 1930–1941. doi:10.1529/biophysj.107.120774. [PubMed: 17993494]

[21]. Ghajar CM, Kachgal S, Kniazeva E, Mori H, Costes SV, George SC, Putnam AJ, Mesenchymal cells stimulate capillary morphogenesis via distinct proteolytic mechanisms, Exp. Cell Res. 316 (2010) 813–825. doi:10.1016/j.yexcr.2010.01.013. [PubMed: 20067788]

[22]. Bayless KJ, Salazar R, Davis GE, RGD-dependent vacuolation and lumen formation observed during endothelial cell morphogenesis in three-dimensional fibrin matrices involves the alpha(v)beta(3) and alpha(5)beta(1) integrins, Am. J. Pathol. 156 (2000) 1673–1683. [PubMed: 10793078]

[23]. Nakatsu MN, Sainson RCA, Aoto JN, Taylor KL, Aitkenhead M, Pérez-del-Pulgar S, Carpenter PM, Hughes CCW, Angiogenic sprouting and capillary lumen formation modeled by human umbilical vein endothelial cells (HUVEC) in fibrin gels: the role of fibroblasts and Angiopoietin-1, Microvasc. Res. 66 (2003) 102–112. [PubMed: 12935768]

[24]. Buno KP, Chen X, Weibel JA, Thiede SN, Garimella SV, Yoder MC, Voytik-Harbin SL, In Vitro Multitissue Interface Model Supports Rapid Vasculogenesis and Mechanistic Study of Vascularization across Tissue Compartments, ACS Appl Mater Interfaces. (2016). doi:10.1021/acsami.6b01194.

[25]. Chung S, Sudo R, Mack PJ, Wan C-R, Vickerman V, Kamm RD, Cell migration into scaffolds under co-culture conditions in a microfluidic platform, Lab Chip. 9 (2009) 269–275. doi:10.1039/b807585a. [PubMed: 19107284]

[26]. Critser PJ, Kreger ST, Voytik-Harbin SL, Yoder MC, Collagen matrix physical properties modulate endothelial colony forming cell-derived vessels in vivo, Microvasc. Res. 80 (2010) 23–30. doi:10.1016/j.mvr.2010.03.001. [PubMed: 20219180]

[27]. Saunders WB, Bohnsack BL, Faske JB, Anthis NJ, Bayless KJ, Hirschi KK, Davis GE, Coregulation of vascular tube stabilization by endothelial cell TIMP-2 and pericyte TIMP-3, J. Cell Biol. 175 (2006) 179–191. doi:10.1083/jcb.200603176. [PubMed: 17030988]

[28]. Cross VL, Zheng Y, Choi NW, Verbridge SS, Sutermaster BA, Bonassar LJ, Fischbach C, Stroock AD, Dense type I collagen matrices that support cellular remodeling and microfabrication for studies of tumor angiogenesis and vasculogenesis in vitro, Biomaterials. 31 (2010) 8596–8607. [PubMed: 20727585]

[29]. Vickerman V, Blundo J, Chung S, Kamm R, Design, fabrication and implementation of a novel multi-parameter control microfluidic platform for three-dimensional cell culture and real-time imaging, Lab on a Chip. 8 (2008) 1468–1477. [PubMed: 18818801]

[30]. Ng CP, Helm C-LE, Swartz MA, Interstitial flow differentially stimulates blood and lymphatic endothelial cell morphogenesis in vitro, Microvasc. Res. 68 (2004) 258–264. doi:10.1016/j.mvr.2004.08.002. [PubMed: 15501245]

[31]. Madri JA, Pratt BM, Tucker AM, Phenotypic modulation of endothelial cells by transforming growth factor-beta depends upon the composition and organization of the extracellular matrix, J. Cell Biol. 106 (1988) 1375–1384. [PubMed: 3283153]

[32]. Koh W, Stratman AN, Sacharidou A, Davis GE, In vitro three dimensional collagen matrix models of endothelial lumen formation during vasculogenesis and angiogenesis, Meth. Enzymol. 443 (2008) 83–101. doi:10.1016/S0076-6879(08)02005-3. [PubMed: 18772012]

[33]. Yang S, Graham J, Kahn JW, Schwartz EA, Gerritsen ME, Functional roles for PECAM-1 (CD31) and VE-cadherin (CD144) in tube assembly and lumen formation in three-dimensional collagen gels, Am. J. Pathol. 155 (1999) 887–895. doi:10.1016/S0002-9440(10)65188-7. [PubMed: 10487846]

[34]. Stratman AN, Malotte KM, Mahan RD, Davis MJ, Davis GE, Pericyte recruitment during vasculogenic tube assembly stimulates endothelial basement membrane matrix formation, Blood. 114 (2009) 5091–5101. doi:10.1182/blood-2009-05-222364. [PubMed: 19822899]

[35]. Kim S, Lee H, Chung M, Jeon NL, Engineering of functional, perfusable 3D microvascular networks on a chip., Lab on a Chip. 13 (2013) 1489. [PubMed: 23440068]

[36]. Park YK, Tu T-Y, Lim SH, Clement IJ, Yang SY, Kamm RD, In Vitro Microvessel Growth and Remodeling within a Three-dimensional Microfluidic Environment, Cellular and Molecular Bioengineering. 7 (2014) 15. [PubMed: 24660039]

[37]. Cuchiara MP, Gould DJ, McHale MK, Dickinson ME, West JL, Integration of Self-Assembled Microvascular Networks with Microfabricated PEG-Based Hydrogels, Adv Funct Mater. 22 (2012) 4511–4518. doi:10.1002/adfm.201200976. [PubMed: 23536744]

[38]. Davis GE, Stratman AN, Sacharidou A, Koh W, Molecular basis for endothelial lumen formation and tubulogenesis during vasculogenesis and angiogenic sprouting, Int Rev Cell Mol Biol. 288 (2011) 101–165. doi:10.1016/B978-0-12-386041-5.00003-0. [PubMed: 21482411]

[39]. Davis GE, Bayless KJ, Mavila A, Molecular basis of endothelial cell morphogenesis in three-dimensional extracellular matrices, Anat. Rec. 268 (2002) 252–275. doi:10.1002/ar.10159. [PubMed: 12382323]

[40]. Bersini S, Yazdi IK, Talò G, Shin SR, Moretti M, Khademhosseini A, Cell-microenvironment interactions and architectures in microvascular systems, Biotechnol. Adv. 34 (2016) 1113–1130. doi:10.1016/j.biotechadv.2016.07.002. [PubMed: 27417066]

[41]. Linville RM, Boland NF, Covarrubias G, Price GM, Tien J, Physical and Chemical Signals That Promote Vascularization of Capillary-Scale Channels, Cell Mol Bioeng. 9 (2016) 73–84. doi:10.1007/s12195-016-0429-8. [PubMed: 27110295]

[42]. Wong KH, Truslow JG, Khankhel AH, Chan KL, Tien J, Artificial lymphatic drainage systems for vascularized microfluidic scaffolds, Journal of Biomedical Materials Research Part A. 101 (2013) 2181–2190. [PubMed: 23281125]

[43]. Sieminski AL, Hebbel RP, Gooch KJ, The relative magnitudes of endothelial force generation and matrix stiffness modulate capillary morphogenesis in vitro, Exp. Cell Res. 297 (2004) 574–584. doi:10.1016/j.yexcr.2004.03.035. [PubMed: 15212957]

[44]. Krishnan L, Underwood CJ, Maas S, Ellis BJ, Kode TC, Hoying JB, Weiss JA, Effect of mechanical boundary conditions on orientation of angiogenic microvessels, Cardiovasc. Res. 78 (2008) 324–332. doi:10.1093/cvr/cvn055. [PubMed: 18310100]

[45]. Edgar LT, Hoying JB, Weiss JA, In Silico Investigation of Angiogenesis with Growth and Stress Generation Coupled to Local Extracellular Matrix Density, Ann Biomed Eng. 43 (2015) 1531–1542. doi:10.1007/s10439-015-1334-3. [PubMed: 25994280]

[46]. Duffy GP, Ahsan T, O'Brien T, Barry F, Nerem RM, Bone marrow-derived mesenchymal stem cells promote angiogenic processes in a time- and dose-dependent manner in vitro, Tissue Eng Part A. 15 (2009) 2459–2470. doi:10.1089/ten.TEA.2008.0341. [PubMed: 19327020]

[47]. Koike N, Fukumura D, Gralla O, Au P, Schechner JS, Jain RK, Tissue engineering: creation of long-lasting blood vessels, Nature. 428 (2004) 138–139. doi:10.1038/428138a. [PubMed: 15014486]

[48]. Bornstein MB, Reconstituted rattail collagen used as substrate for tissue cultures on coverslips in Maximow slides and roller tubes, Lab. Invest. 7 (1958) 134–137. [PubMed: 13540204]

[49]. Rajan N, Habermehl J, Coté M-F, Doillon CJ, Mantovani D, Preparation of ready-to-use, storable and reconstituted type I collagen from rat tail tendon for tissue engineering applications, Nat Protoc. 1 (2006) 2753–2758. doi:10.1038/nprot.2006.430. [PubMed: 17406532]

[50]. Yang Y-L, Leone LM, Kaufman LJ, Elastic moduli of collagen gels can be predicted from two-dimensional confocal microscopy, Biophys. J. 97 (2009) 2051–2060. doi:10.1016/j.bpj.2009.07.035. [PubMed: 19804737]

[51]. Wu C-C, Ding S-J, Wang Y-H, Tang M-J, Chang H-C, Mechanical properties of collagen gels derived from rats of different ages, J Biomater Sci Polym Ed. 16 (2005) 1261–1275. [PubMed: 16268252]

[52]. Zuidema JM, Rivet CJ, Gilbert RJ, Morrison FA, A protocol for rheological characterization of hydrogels for tissue engineering strategies, J. Biomed. Mater. Res. Part B Appl. Biomater. 102 (2014) 1063–1073. doi:10.1002/jbm.b.33088. [PubMed: 24357498]

[53]. Bala K, Ambwani K, Gohil NK, Effect of different mitogens and serum concentration on HUVEC morphology and characteristics: implication on use of higher passage cells, Tissue Cell. 43 (2011) 216–222. doi:10.1016/j.tice.2011.03.004. [PubMed: 21511321]

[54]. Liao H, He H, Chen Y, Zeng F, Huang J, Wu L, Chen Y, Effects of long-term serial cell passaging on cell spreading, migration, and cell-surface ultrastructures of cultured vascular endothelial cells, Cytotechnology. 66 (2014) 229–238. doi:10.1007/s10616-013-9560-8. [PubMed: 23553018]

[55]. Kovesi P, Phase Preserving Denoising of Images, n.d.

[56]. Vincent L, Morphological grayscale reconstruction in image analysis: applications and efficient algorithms, IEEE Trans Image Process. 2 (1993) 176–201. doi:10.1109/83.217222. [PubMed: 18296207]

[57]. Xie L, Sparks MA, Li W, Qi Y, Liu C, Coffman TM, Johnson GA, Quantitative susceptibility mapping of kidney inflammation and fibrosis in type 1 angiotensin receptor-deficient mice, NMR Biomed. 26 (2013) 1853–1863. doi:10.1002/nbm.3039. [PubMed: 24154952]

[58]. Van Uitert R, Bitter I, Subvoxel precise skeletons of volumetric data based on fast marching methods, Med Phys. 34 (2007) 627–638. doi:10.1118/1.2409238. [PubMed: 17388180]

[59]. Serra R, Rizzuto A, Rossi A, Perri P, Barbetta A, Abdalla K, Caroleo S, Longo C, Amantea B, Sammarco G, de Franciscis S, Skin grafting for the treatment of chronic leg ulcers - a systematic review in evidence-based medicine, Int Wound J. 14 (2017) 149–157. doi:10.1111/iwj.12575. [PubMed: 26940940]

[60]. Cheema U, Rong Z, Kirresh O, Macrobert AJ, Vadgama P, Brown RA, Oxygen diffusion through collagen scaffolds at defined densities: implications for cell survival in tissue models, J Tissue Eng Regen Med. 6 (2012) 77–84. doi:10.1002/term.402. [PubMed: 21312340]

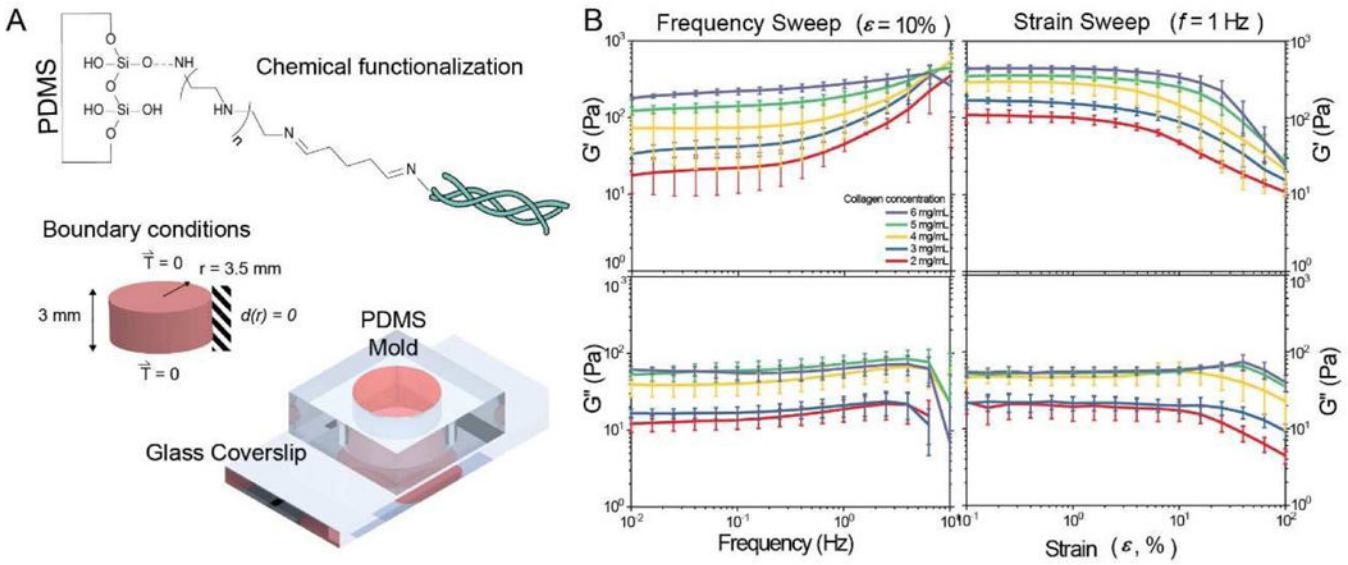

Figure 1: Collagen well/mold geometry and rheological characterization.

(A) Cartoon of gel/mold fabrication. For three-dimensional culture of cells, collagen was gelled in a cylindrical PDMS mold chemically functionalized to adhere collagen. The upper and lower surfaces were free to slip, while PEI/GA functionalization was used to fix the circumferential boundary. The mold was placed on coverslip glass to allow for high resolution imaging. (B) Rheological characterization (frequency sweep; ε = 10%, left and strain sweep; f =1 Hz, right) was performed on collagen gels with collagen concentrations that match those used in our studies. Data presented as mean ± S.E.M (n = 2-4).

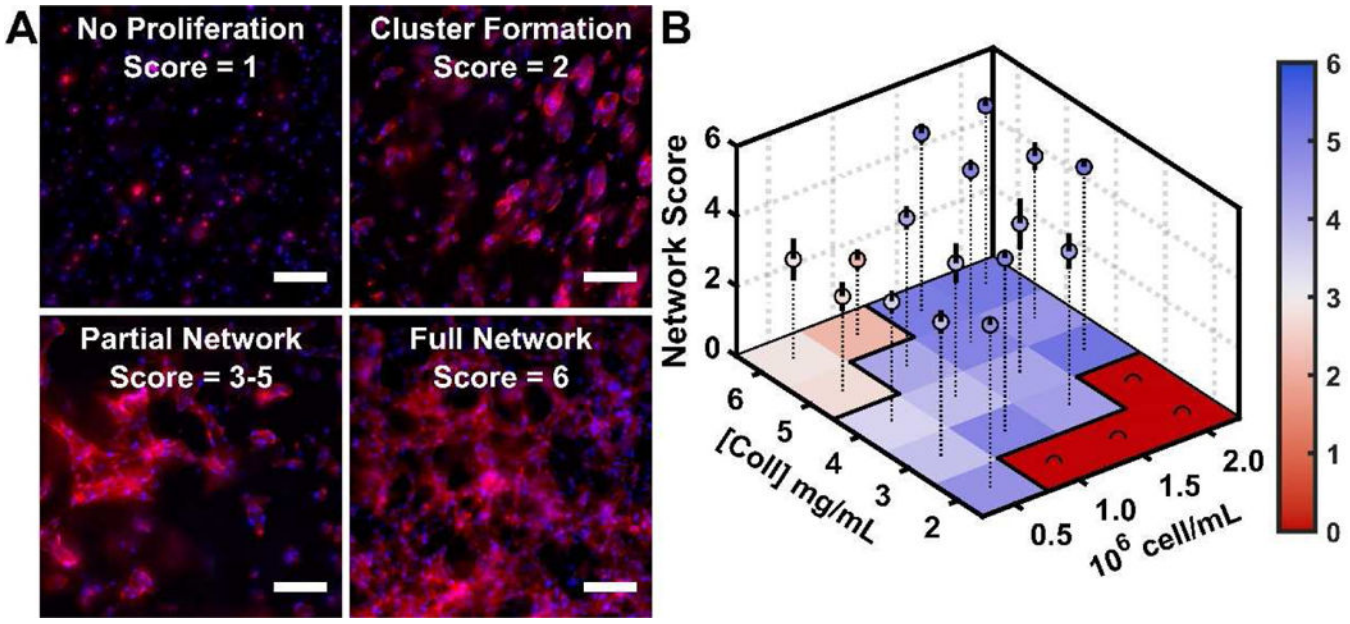

Figure 2: Effect of cell and collagen densities on vascular network quality.

HUVECs were cultured in 3D collagen gels for 7 days at a range of collagen densities ([Coll]; mg/mL) and cell concentrations (10^6 cell/mL). Cells were fixed and stained with phalloidin (to label the F-actin cytoskeleton; red) and DAPI (to label nuclei; blue). (A) Representative images of observed higher-order behaviors. Example images of the observed subjective phenotypes, with associated score. In the case of "Partial Network" the score varies from 3-5 depending on the approximate percentage of network coverage (25, 50, or 75%). Images are maximum projections of z-stacks with background subtraction for clarity. Scale bars 200 μm. (B) Qualitative assessment of network formation over a range of culture conditions. Robust network formation occurs along an axis of increasing cell and collagen density. Network Score is shown colorimetrically as mean ± S.E.M. ("between observer"; n≥3).

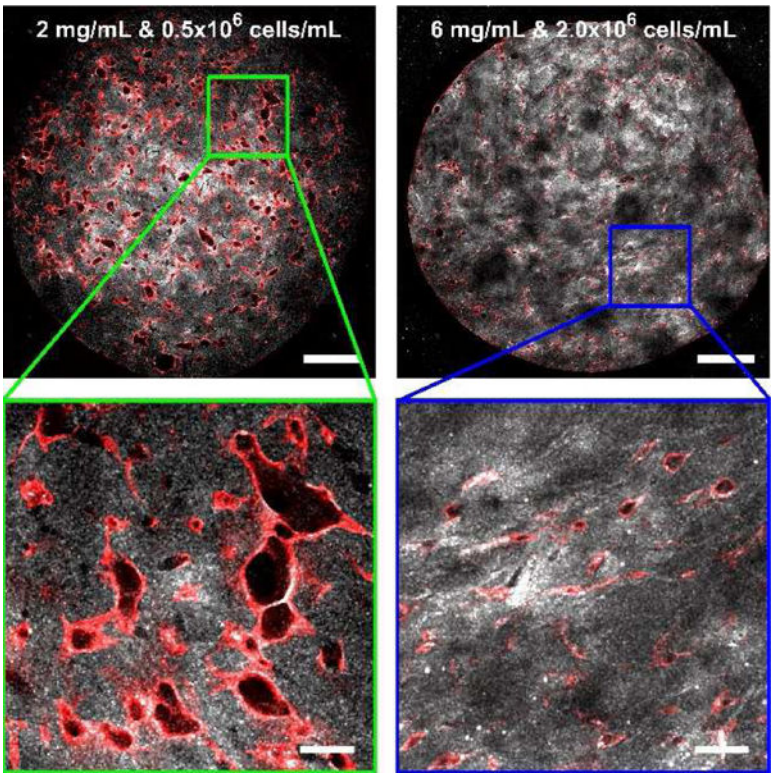

Figure 3: Culture conditions result in distinct differences in vascular network morphology.

A subset of HUVEC/Collagen gels prepared above were imaged as a confocal volume. HUVECs were labeled with phalloidin (red) and confocal reflectance (white) was used to localize collagen. Confocal planes from two example culture conditions are shown. Regions highlighted with green and blue squares in top images correspond to zoom images below. The lower collagen and cell densities resulted in networks with larger lumens, whereas the networks in the gels with higher collagen and cell densities exhibited thinner, more intricate networks. Images were median filtered for clarity. Scale bars are 1 mm (full images; top) and 200 μm (zoom images; bottom).

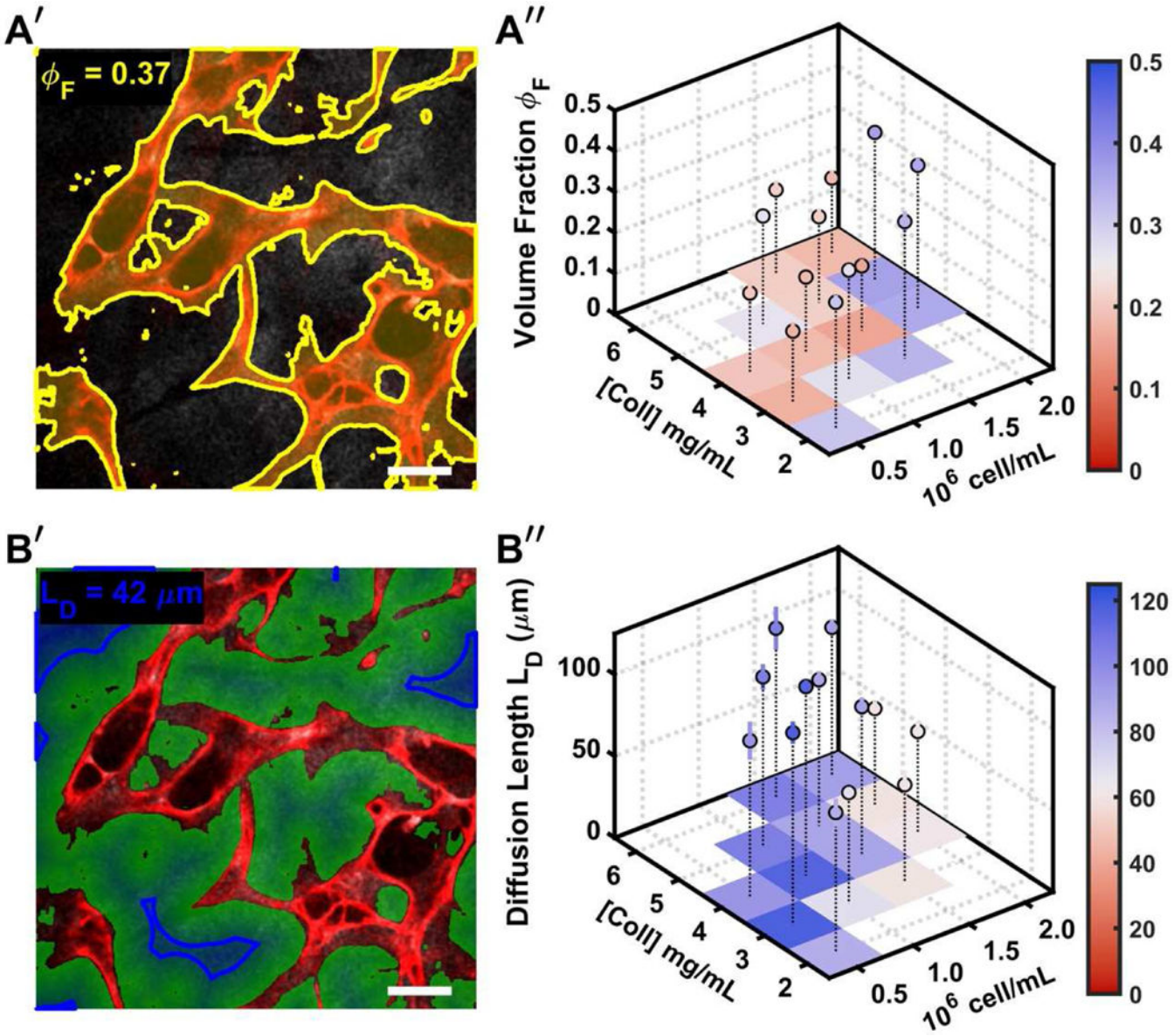

Figure 4: Softer gels and more cells lead to increasing volume fraction of vessels and decreasing diffusion length.

HUVECs were cultured in 3D collagen gels for 7 days in the range of collagen densities ([Coll]; mg/mL) and cell concentrations (10^6 cell/mL) that qualitatively resulted in robust network formation. (A') The volume fraction (ϕ_F) is shown schematically on an example confocal region. The area shaded yellow represents the network, and a volume fraction for the example region is shown for display purposes only. (A") There is a trend of increasing ϕ_F in softer gels and increasing cell concentration. (B') To approximate diffusion length, L_D, we determined the 90th percentile of distance from the network, indicated in an example confocal region by a blue line. Distance from the network is indicated by green fading to blue with increasing distance. (B") L_D is consistent with the trends for ϕ_F, in softer gels and increasing cell concentration. Volume fraction and diffusion distance are shown colorimetrically as mean ± S.E.M. (n=5-31).

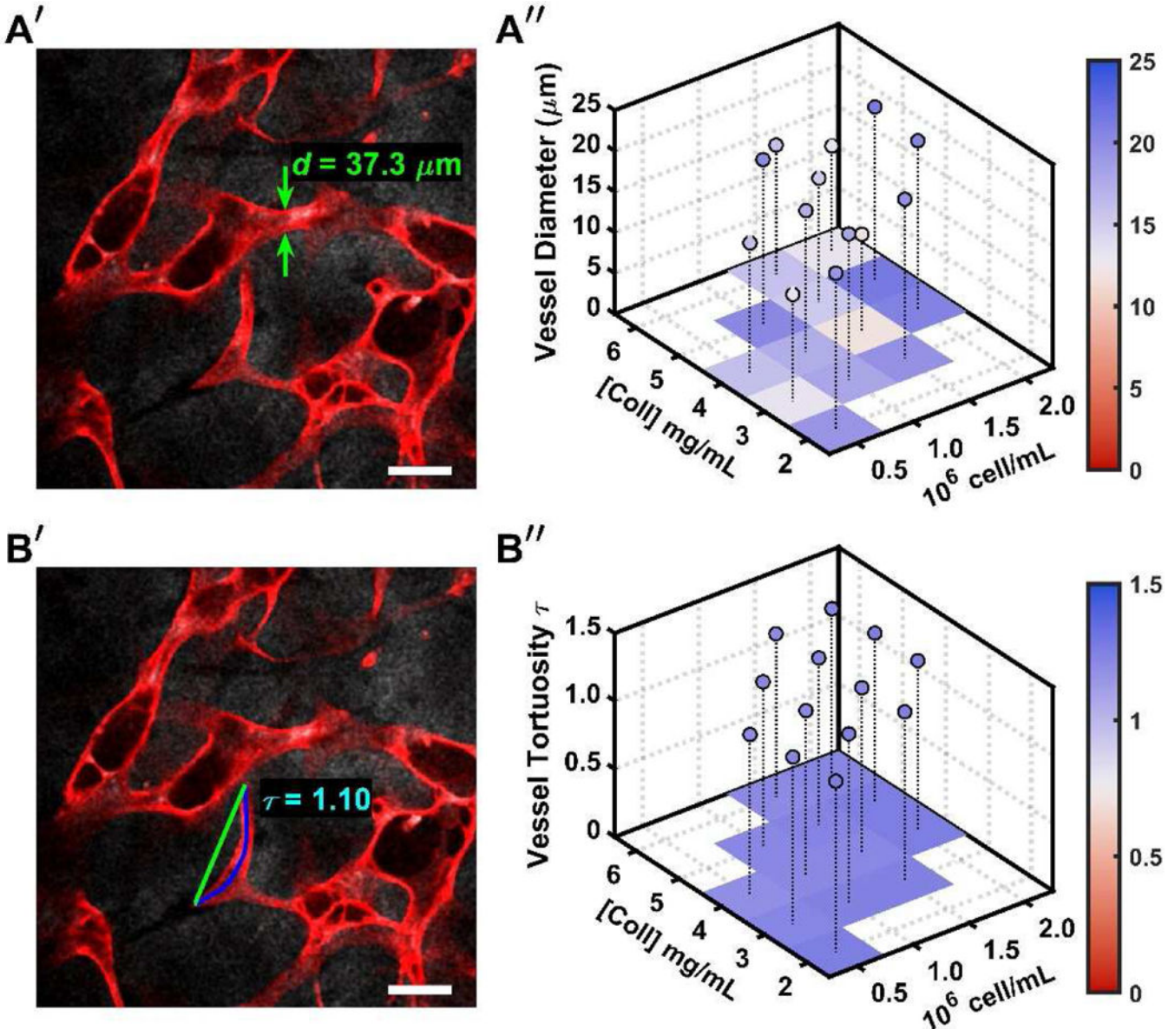

Figure 5: Networks are composed of minimally tortuous segments averaging 10-25 μ m.

HUVECs were cultured in 3D collagen gels for 7 days in the range of collagen densities ([Coll]; mg/mL) and cell concentrations (10^6 cell/mL) that qualitatively resulted in robust network formation. (A') We measured the diameter of individual segments, shown schematically as an example. (A") In all cases, average segment diameter was between 10-30 μm. (B') We additionally measured tortuosity (τ), defined as length (blue) divided by the chord (green) of a network segment. (B") Regardless of culture condition, network segments are relatively straight (average $\tau > 0.8$ for all cases). Network segment diameter and tortuosity are shown colorimetrically as mean ± S.E.M. (n=5-31).

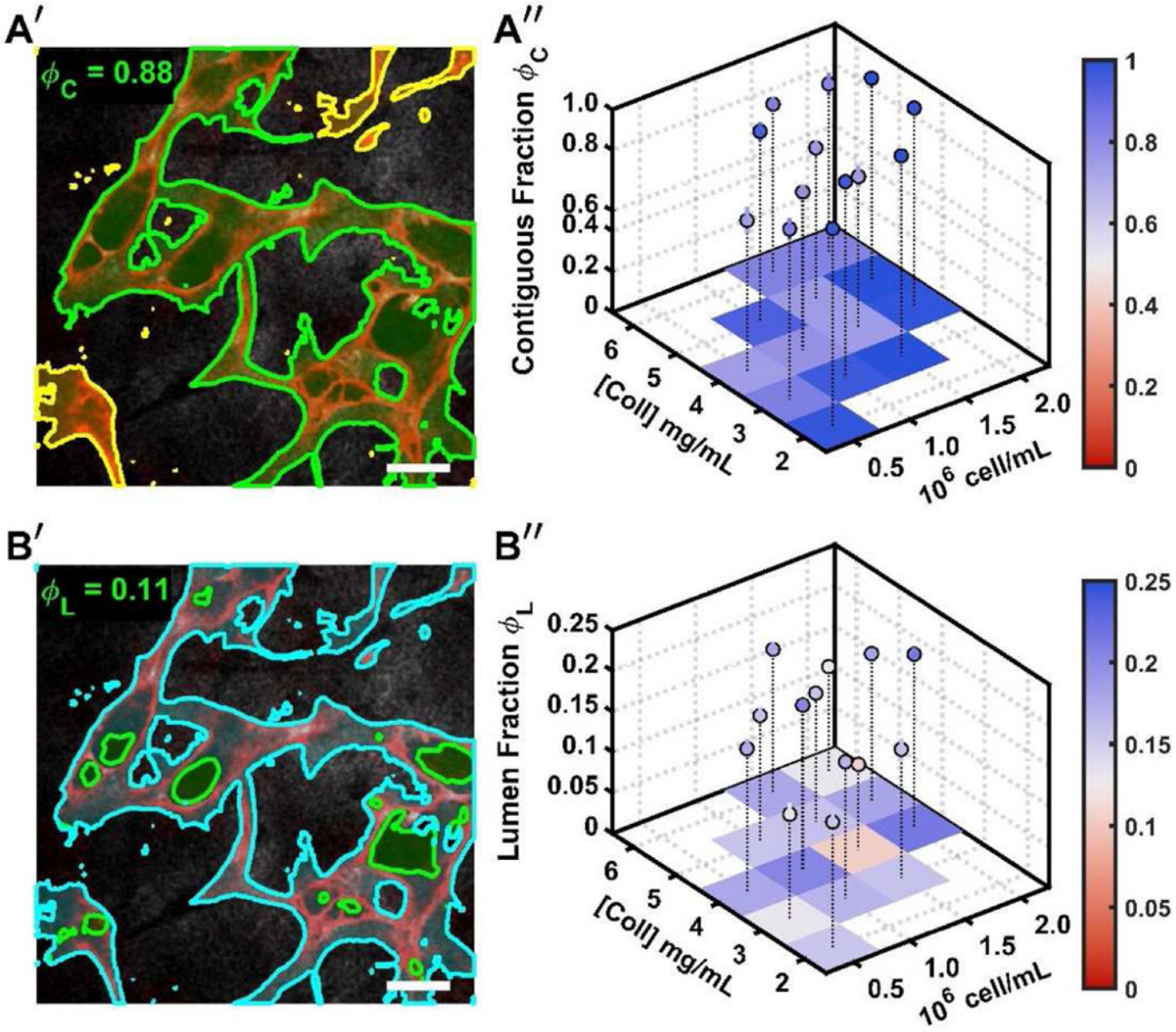

Figure 6: Lower collagen densities result in a connected network, and networks are consistently lumenized in all conditions.

HUVECs were cultured in 3D collagen gels for 7 days in the range of collagen densities ([Coll]; mg/mL) and cell concentrations (10^6 cell/mL) that qualitatively resulted in robust network formation. (A') We determined the largest contiguous fraction of the network (ϕ_C) as a measure of network connectivity in three dimensions. As an example, this is shown schematically in two dimensions. The large contiguous region is green, while the disconnected regions are yellow. (A") In all tested conditions, there was a high (>50%) level of connectivity, and lower collagen densities trended towards higher connectivity. (B') Additionally, by sub-dividing the network into cell (cyan) and lumen (green) fractions, we can approximate the amount of the network that possesses lumens. (B") There was a consistent level of lumenization of ~20-30% throughout all culture conditions. Contiguous Fraction and Lumen Fraction are shown colorimetrically as mean ± S.E.M. (n=5-31).

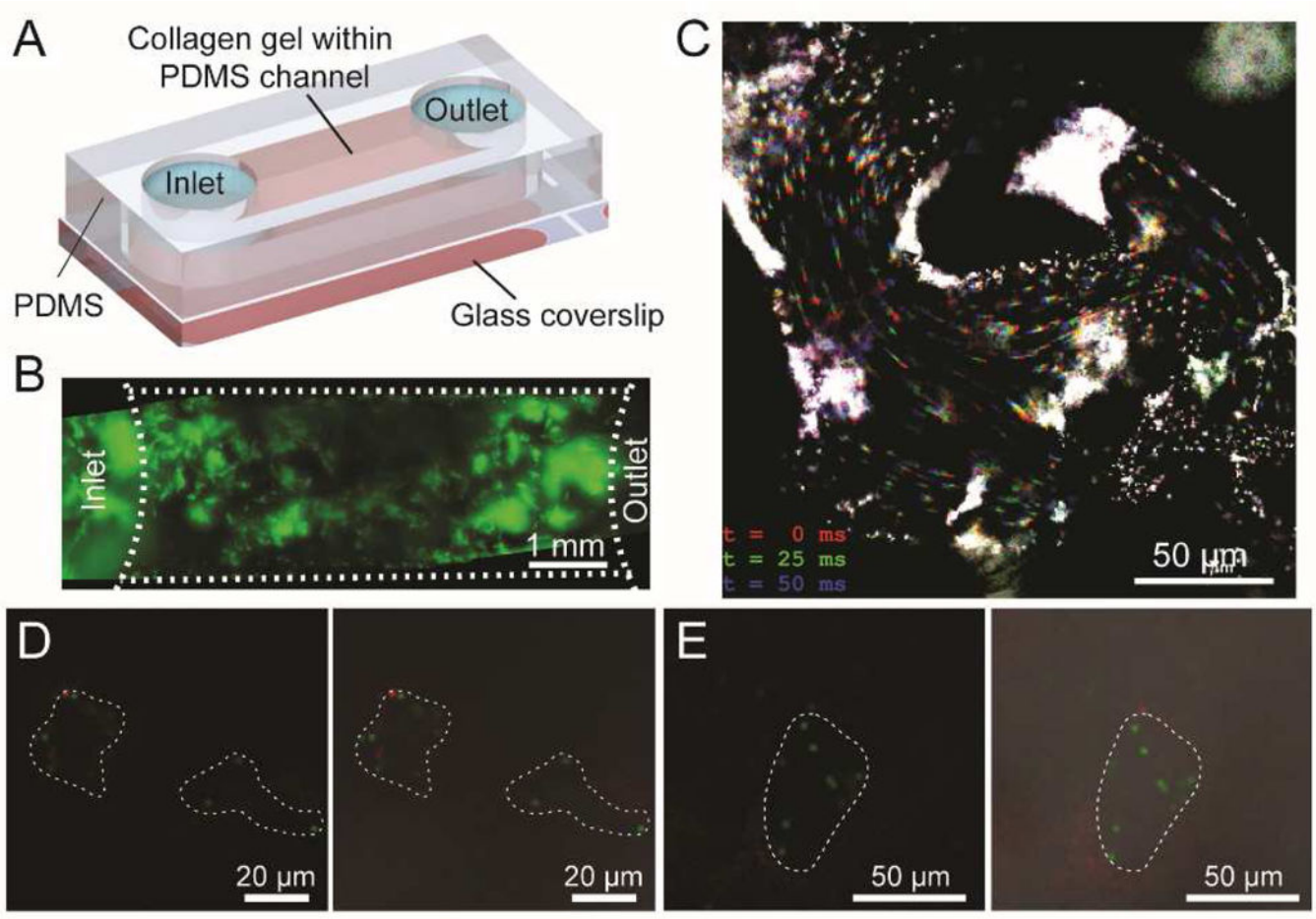

Figure 7: Engineered vasculatures have patent lumens and support perfusion throughout their networks.

(A) Perfusion studies were conducted in a PDMS glass device with inlet and outlet ports for perfusion of the self-assembled vascular network. (B) Example perfusion results across the entire construct (1.0×10^6 cell/mL embedded in 4 mg/mL collagen) following perfusion with 500nm fluorescent microspheres (green). (C) Live imaging of microsphere flow through a vessel junction in overlaid stills (red: t=0 ms; green: t=25 ms; blue: t=50 ms). Stationary beads adhered to the endothelial cells show up as white streaks bordering the flow. White dots in the upper right and lower left represent beads moving normal to the imaging plane, indicating the three-dimensional nature of the convective flow. (D,E) Example data from self-assembled vascular networks following 14 days of culture at different cell densities and collagen concentrations. Shown are single confocal slices within these constructs following perfusion of 2mm fluorescent microspheres (green) (fluorescence image with HUVECs (red), left; fluorescence and DIC overlay, right). Vessel lumens are traced with dotted white lines. Collectively, these data demonstrate successful perfusion of fluorescent microspheres within large (C) and small diameter vascular lumens (D,E).

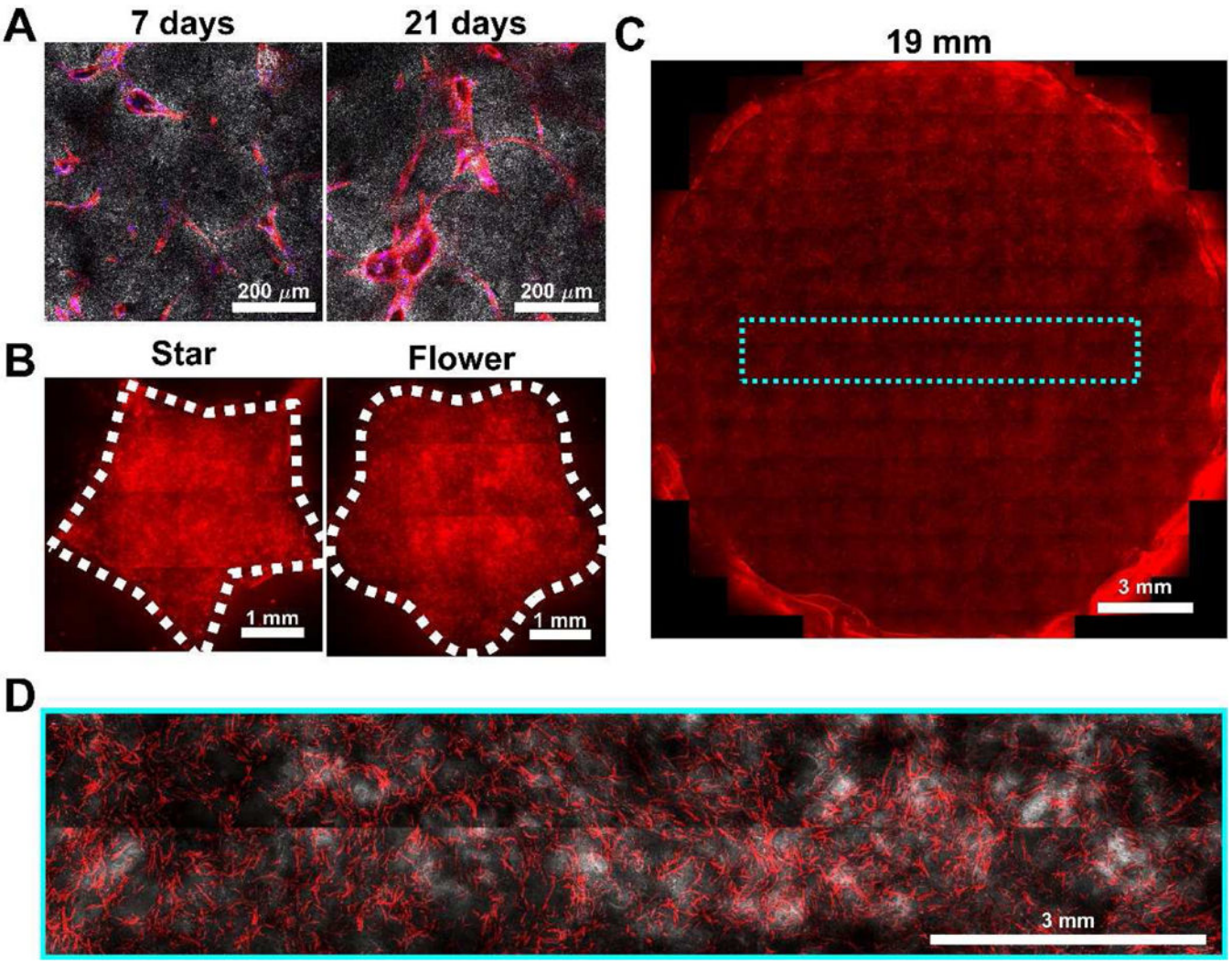

Figure 8: Plexus formation is robust with extended culture and formation in centimeter-scale sizes and arbitrary geometries.

HUVECs were embedded in 5 mg/mL collagen at 1.5×10^6 cell/mL. (A) Using the 7 mm culture format used in prior experiments, HUVECs from a single passage were cultured for 7, 14 (not shown), and 21 days before fixation, phalloidin (red) and DAPI (blue) staining, and confocal imaging. At all time points, HUVECs presented similar network morphologies and clear lumens. (B) HUVECs were grown for 7 days in alternatively shaped plexus molds including star and flower shapes. In all shapes, HUVECs presented similar network morphologies and a formed a vascular network into both large and small curvatures of the mold boundaries (flower and star respectively, max projection images). (C-D) HUVECs were grown in 19 mm diameter (3 mm thick) molds for 7 days before fixation, phalloidin staining, and (C) epifluorescent (image shown is of 1 mm max projection) or (D) confocal imaging (image shown is of 300 μm max projection). Even at this scale, HUVECs formed qualitatively similar network morphologies to smaller collagen gels. Dotted cyan box in (C) corresponds roughly to the position and size of the confocal volume shown in (D).